



## Chemically heterogeneous nitrogen sites of various reactivity in porous carbons provide high stability of CO<sub>2</sub> electroreduction catalysts



Wanlu Li<sup>a,b</sup>, Nina Fechler<sup>c</sup>, Teresa J. Bandosz<sup>a,b,\*</sup>

<sup>a</sup> Department of Chemistry and Biochemistry, The City College of New York, New York, NY, 10031, USA

<sup>b</sup> Ph.D. Program in Chemistry, The Graduate Center of the City University of New York, New York, NY, 10016, USA

<sup>c</sup> Max Planck Institute of Colloids and Interfaces, Department of Colloid Chemistry Research Campus Golm, Potsdam, 14476, Germany

### ARTICLE INFO

#### Keywords:

N-doped microporous carbon  
CO<sub>2</sub>  
Reduction  
Surface chemistry  
Catalyst stability  
Hydrocarbon formation

### ABSTRACT

Microporous carbons of high nitrogen-content and diverse nitrogen-doping sites were studied for CO<sub>2</sub> electrochemical reduction. The unique feature of these carbon materials is the presence of chemically heterogeneous nitrogen species of various reactivity. The systematic surface chemistry study reveals that some nitrogen moiety, even though it has no direct catalytic role in the CO formation during CO<sub>2</sub> reduction process, protects the active pyridinic nitrogen from oxidation. In that protection mechanism, these species, instead of pyridines, are oxidized. Therefore, that nitrogen is believed to be responsible for the exceptional stability of the carbon catalysts found in this study. Besides CO and CH<sub>4</sub>, methanol, formic acid and C<sub>3</sub> hydrocarbons (acetone and propanol) were also detected as reduction products. C<sub>3</sub> hydrocarbons are the first reported products among the metal-free catalysts for CO<sub>2</sub> reduction. The results suggest that the C<sub>3</sub> products could be formed when more than one nitrogen sites are located close to each other in the pore space. Furthermore, the differences in the porosity suggest that the microporous structure of the carbons favors the hydrocarbons formation. Eventually, the carbons described herein offer a unique combination of chemical and physical properties, which give further insights into the electrochemical reduction of CO<sub>2</sub> on functional carbon materials.

### 1. Introduction

Carbon-based materials have become subject of studies as catalysts for the CO<sub>2</sub> electrochemical reduction (CO<sub>2</sub>ERR) in the recent five years [1–5]. Their catalytic activity is linked to the defects in the carbon matrices. Nitrogen has been indicated as one of the most influential doping elements, which can enhance CO<sub>2</sub>ERR [1–5]. The study of nitrogen-doped carbon nanotubes [2] showed that the quaternary and pyridinic nitrogen sites significantly decrease the overpotential and increase the Faradaic efficiency (FE) for CO. The reported FE for the CO formation was 80% at –1.1 V vs. SCE (with 1.1% atomic concentration (at.) of pyridinic nitrogen and 3.5% atomic concentration of graphitic nitrogen). Nitrogen-doped graphene [5] with 3 at. % pyridinic-nitrogen and 1.8 at. % graphitic nitrogen was also studied as an electrocatalyst converting CO<sub>2</sub> to formate with a FE of 73% at the potential of –0.84 V vs. RHE.

Apart from those nanoforms of carbons, our recent efforts have focused on nanoporous carbons. This is based on the possible enhancement in the catalytic activity due to their high surface area and advantageous pore structure. Not without importance is that distorted

graphene layers arranged in a random way constitute the pore structure of these materials. In addition, costs and synthetic requirements of (nano)porous carbons are much lower than those of nanocarbons. On dual-doped (S- and N-) nanoporous carbon derived from polymers [6], the FE of CO formation reached 11% with a trace amount of CH<sub>4</sub> detected at –0.99 V vs. RHE. The results suggested that nitrogen functionalities are more active for CO<sub>2</sub>ERR than sulfur sites. For example, for a wood-based electrochemically reduced form of N-doped nanoporous carbon the FE for CO and CH<sub>4</sub> formation were 39% and 1.2%, respectively. The results support the previous finding [7] that pyridinic-N is the most active site for CO<sub>2</sub>ERR among all the nitrogen-containing functional groups present on the surface of those particular carbons. The amount of CH<sub>4</sub> formed on the nanoporous carbons was directly related to the amount of CO formed. Besides, the surface basicity and a high volume of ultramicropores improved the CO<sub>2</sub> reduction process. Recent results implied that the nanoporous structure might be crucial for the CH<sub>4</sub> formation [7]. It was suggested that the ultramicropores function as Fisher-Tropsch nanoreactors in which methane is formed owing to a strong adsorption of CO and an involvement of hydrogen from water splitting.

\* Corresponding author at: Department of Chemistry and Biochemistry, The City College of New York, New York, NY, 10031, USA.  
E-mail address: [tbandosz@ccny.cuny.edu](mailto:tbandosz@ccny.cuny.edu) (T.J. Bandosz).

Besides a high Faradaic efficiency, a catalyst stability is one of the most important requirements for efficient CO<sub>2</sub>ERR. Many reports show that polycrystalline or nanostructured metal catalysts were deactivated within a minute timescale [8]. On an Ag nanostructure catalyst a high FE of 80% for CO at the −0.50 V vs. RHE was reported, however, it only lasted for 8 h [9]. Nitrogen-doped carbon nanofibers provided a stable current density for 9 h at 0.57 V vs. RHE [1]. An N-graphene catalyst showed a stability of 12 h towards the formate formation with a FE of 70% at −0.84 V vs. RHE [5]. On the other hand, the FE for CO formation on nitrogen-doped wood-based porous carbon decreased from 39% to 20% after 24 h and to 15% after 48 h reduction, respectively [7]. Since instability is a crucial parameter limiting catalyst applications, there is an urgent need to develop stable catalysts.

Regarding the catalytic sites, the roles of pyridinic and quaternary (graphitic) nitrogen configurations inside the carbon structure for CO<sub>2</sub>ERR are still under debate, however, there is an indication of their activity [1–7]. Our results reported suggest that the pyridinic nitrogen configuration is of paramount importance for the CO formation [6,7]. Based on this, another configuration, pyrazinic nitrogen, gained our attention since its structure is very similar to the active pyridinic-N sites. Besides providing double the amount of nitrogen per ring unit in comparison to pyridinic-N, pyrazinic-N might also affect the mechanism of the reduction process owing to the close proximity of these two N-bonds in this particular chemical species. Up to now, very little is known about the role of this configuration in CO<sub>2</sub>ERR as the carbon with pyrazinic-N has been synthesized only recently [10,11]. Moreover, a clear identification of pyrazinic nitrogen in the carbon is very difficult owing to the overlapping of its binding energy with that of pyridines [10]. Therefore, a series of microporous carbons containing heterogeneous nitrogen configurations including a significant contribution of nitrogen in electrochemical stable pyridines were synthesized and tested as CO<sub>2</sub> electroreduction catalysts. The objective of this paper is to evaluate the influence N-species chemical heterogeneity in the microporous carbon matrix on CO<sub>2</sub>ERR. Initial samples as well as those exposed to CO<sub>2</sub>ERR were extensively analyzed with regard to the acidity/basicity, porous structure, and the changes/trends in surface features of catalysts caused upon the participation in hydrogen evolution reaction (HER) and CO<sub>2</sub>ERR. Based on the trends, the role of different structural N-configurations in microporous carbons, in affecting the catalytic efficiency is proposed. Our objective is to show that specifically designed surface chemistry can provide the long-term stability of the catalyst, which is a desired feature compensating a not-very-high Faradaic efficiency.

## 2. Experimental procedures

### 2.1. Materials

Urea (Aldrich, 98%) and Squaric acid (Aldrich, 98.5%) were used as received without further purification. Squaric acid, urea (molar ratio 1:2) and ZnCl<sub>2</sub> (weight ratio squaric acid/urea-mixture: ZnCl<sub>2</sub> 1:1) were ground in a mortar. The homogenous mixture was then transferred into a ceramic crucible and heated to 700, 800, and 900 °C under N<sub>2</sub> atmosphere with a heating ramp of 2.5 K/min using a Nabertherm N7/H chamber oven with a P300 controller. The final temperature was kept for 1 h. After carbonization, the products were grinded and stirred overnight in 1 M HCl, filtered, washed several times with water and then with ethanol and finally dried in a vacuum oven (60 °C).

### 2.2. Methods

#### 2.2.1. CO<sub>2</sub> electrochemical reduction

To prepare a working electrode, a homogeneous slurry of an active material with polyvinylidene fluoride (PVDF) and carbon black (CB) (mass ratio 8:1:1) in N-methyl-2-pyrrolidone (NMP) was first prepared. Carbon black was added to increase the electrode conductivity. A

uniform 5 ± 0.2 mg/cm<sup>2</sup> catalyst was coated double sides on to a Titanium (Ti) foil (1 cm<sup>2</sup>). Such prepared electrodes were dried at 100 °C overnight in an oven. Since the Ti foil was fully covered by a layer of the catalyst, it was assumed that the current generated on Ti does not affect our results in a marked way.

The CO<sub>2</sub>ERR was evaluated at different reduction potentials in CO<sub>2</sub> (ultrapure 99.99%) saturated KHCO<sub>3</sub> electrolyte (0.1 M) on VersaSTAT MC (AMETEK, Princeton Applied Research). The tests were performed in an airtight three-electrode and two compartments cell separated by a cation exchange membrane (Nafion 117). Ag/AgCl/NaCl (3 M) was used as a reference electrode and Pt wire as a counter electrode. The resistance of the electrochemical cell was measured before experiment using IR compensation. A measured cell resistance was approximately 40 Ω on all the catalyst samples. After the testing, the data were corrected to remove 100% of the cell resistance. Before the electrochemical CO<sub>2</sub> reduction reaction, the electrodes were wetted in KHCO<sub>3</sub> (0.1 M) for 4 h with an open circuit voltage (OCV) vs. Ag/AgCl was recorded. Then the cyclic voltammetry (CV) experiments were run in the potential window from 0 V to −1.5 V vs. Ag/AgCl to test the stability with an increase in the number of cycles. The OCV and CV measurements were performed in a N<sub>2</sub>-saturated electrolyte. Potential values are reported versus reversible hydrogen electrode (RHE): E (vs. RHE) = E (vs. Ag/AgCl) + 0.21 V + 0.059 × pH (pH of saturated CO<sub>2</sub> 0.1 M KHCO<sub>3</sub> is 6.8). Before CO<sub>2</sub>ERR, the electrolyte was purged with CO<sub>2</sub> for 30 min and headspace of the cell for 20 min. Then the chronoamperometry (CA) was run under constant potentials between −0.3 V and −1.2 V vs. RHE for 6 h. During the CA run, the gas phase products from the headspace of the cathodic compartment of the electrochemical cell were analyzed every hour using gas chromatograph (GC) (model SRI 8610 C). The gas phase was injected into the GC column using a gas-tight syringe and the separation was done on a carboxen column (Carboxen-1000, 4.57 m in length, and 2.1 mm in internal diameter). The GC oven heating program was as follows: 35 °C for 5 min, then heating from 35 to 220 °C at a rate of 20 °C/min and holding at 220 °C for 5 min. The carrier gas was He with a flow rate of 30 mL/min. A flame ionization detector (FID) was used to detect hydrocarbons, and a thermal conductivity detector (TCD). CO, CH<sub>4</sub> and H<sub>2</sub> were the target reduction products. Even though the concentration of CH<sub>4</sub> was very small, it was in the range of the amount used to calibrate the detector ( $R^2 = 0.992$ ). Additionally, the content of the electrolyte solution after 48 h CO<sub>2</sub>ERR was tested using NMR. <sup>1</sup>H NMR data were acquired at 298 K on a Bruker 800 MHz Advance III HD spectrometer equipped with a 5-mm TCI cryoprobe. 1D <sup>1</sup>H NMR spectra were recorded with a sweep of 16 ppm centered on the water, 1.7 s acquisition time, 2 s relaxation delay, gradient excitation sculpting water suppression, for the total of 512 scans.

The samples tested in CO<sub>2</sub>ERR have an additional letter “E” is added to their names. The sample reduced for 48 h in the N<sub>2</sub> saturated electrolyte is designated with an additional “N<sub>2</sub>” is added to its name.

Control experiments were carried out on the carbon electrode without the presence of CO<sub>2</sub> in the system (to test the release of CO and CH<sub>4</sub> as a result of carbon decomposition) and on bare titanium foil with CO<sub>2</sub> in the system (to check the effect of the current collector on CO<sub>2</sub> reduction).

#### 2.2.2. Characterization of the catalysts

**2.2.2.1. Adsorption of nitrogen.** Adsorption of nitrogen was measured on ASAP 2020 Surface Area and Porosity Analyzer (Micromeritics) at −196 °C. Before each analysis, the samples were outgassed at 120 °C to constant vacuum ( $10^{-4}$  Torr). At these conditions only physically adsorbed species were removed without changing the surface chemistry. The surface areas (NLDFT method), total pore volumes (V<sub>t</sub>), the volumes of mesopore (V<sub>meso</sub>), micropore (V<sub>mic</sub>), ultramicropore (V<sub><0.7 nm</sub>) and the volume of pores smaller than 1 nm (V<sub><1 nm</sub>), were calculated from the isotherms. The volumes of pores and pore size distributions were calculated using the Non-Linear

Density Functional Theory (NLDFT) [www.nldft.com](http://www.nldft.com) [12].

**2.2.2.2. Resistance measurements.** A film of a sample dispersed in N-methyl-2-pyrrolidone was coated on a 0.5 cm × 0.45 cm gold interdigitated electrode. The samples were dried at 120 °C for 24 h. The sheet resistance was measured with a 4-probe method using Keithley 2400 Multimeter. The thickness of the sample was around 100 µm.

**2.2.2.3. Potentiometric titration.** Potentiometric titration analysis was carried out on a DMS Titrando 888 automatic titrator (Metrohm). The samples (~0.050 g) were added to 25 mL of NaNO<sub>3</sub> (0.01 M), and equilibrated overnight at a room temperature. The suspension was saturated with N<sub>2</sub> throughout the measurements under a continuous stirring to eliminate the influence of atmospheric CO<sub>2</sub>. Each sample was titrated with volumetric standard NaOH (0.1 M) after adding 0.1 M HCl to the sample suspension. The initial pH of the suspension was discussed as the surface pH value. The experimental data were transformed into proton binding curves, Q, and then to pK<sub>a</sub> distributions. The pK<sub>a</sub> distributions were calculated using SAIEUS numerical procedure [12,13].

**2.2.2.4. X-ray photoelectron spectroscopy (XPS).** The XPS spectra were collected using the Physical Electronics PHI 5000 VersaProbe II spectrometer with a monochromatic Al K $\alpha$  (1486.6 eV) radiation operating at 15 kV and 50 W in the analyzer chamber. Prior to analysis, all samples were outgassed until 10<sup>-8</sup> Torr at room temperature. High-resolution spectra of powdered samples were detected with the constant pass energy values of 29.35 eV and a 200 µm diameter analysis area with a take-off angle of 45°. 117.4 eV pass energy was used for the survey spectra. The detailed amounts of each element were calculated from the individual spectra. The spectrometer energy scale was calibrated using Cu 2p<sub>3/2</sub>, Ag 3d<sub>5/2</sub>, and Au 4f<sub>7/2</sub> photoelectron lines at 932.7, 368.3, and 84.0 eV, respectively. The SmartSoft-VP2.6.3.4 software package was used for acquisition and data analysis and Multipack software was used to fit photoelectron spectra. A Shirley-type background was subtracted from the signals and recorded spectra were fitted using Gauss–Lorentz curves in order to determine the binding energy of the different element core levels accurately.

### 3. Results and discussion

#### 3.1. CO<sub>2</sub> electrochemical reduction activity

The carbons used as catalysts in this study (SaU-700, SaU-800 and SaU-900, where the numbers refer to the synthesis temperature) were synthesized from pre-organized precursors of squaric acid and urea in a salt melt. Fig. 1a and b show the trends in FE for CO and CH<sub>4</sub> at various

potentials at the 6 h reduction process. CO was the main reaction product of CO<sub>2</sub>ERR. SaU-900 catalyzed the CO formation starting at –0.37 V vs. RHE, corresponding to the overpotential of 0.26 V. The potential at which either CO or CH<sub>4</sub> was first detected is considered here as an onset potential for the specific species. The onset potential of CO formation on SaU-900 is shifted to the more positive value when compared to that for the dual-doped (S- and N-) polymer-derived carbon (–0.59 V vs. RHE) studied previously [6]. A very similar value was measured on wood-based carbon modified with melamine (–0.36 V vs. RHE) [7]. The FE for CO formation on SaU-900 reached 21% at –0.75 V vs. RHE and 22% at –0.85 V vs. RHE, respectively. At more negative potentials the FE of CO formation decreased. This is linked to the higher extent of hydrogen evolution reaction (HER) than that of CO<sub>2</sub>ERR [9,14].

CH<sub>4</sub> was formed with a maximum FE of 0.35% at –1.0 V vs. RHE. The trend in the efficiency of CH<sub>4</sub> formation on SaU-900 at the various potentials was similar to that for CO. For SaU-800, the onset potential for both CO and CH<sub>4</sub> formation was 100 mV more negative than those on SaU-900. FE of CO at its maximum (at –0.75 V vs. RHE) was also smaller than that on SaU-900 at the same potential. However, both SaU-800 and SaU-900 displayed similar FEs for the CH<sub>4</sub> formation at a potential range from –0.5 to –0.9 V vs. RHE. At –0.75 V, FE of CH<sub>4</sub> was even higher on SaU-800 than that on SaU-900. The ratio of FE for CH<sub>4</sub> to that for CO clearly indicates that SaU-800 favors CH<sub>4</sub> formation. On the other hand, SaU-700 showed a very poor Faradaic efficiency for both CO and CH<sub>4</sub> formations. Overall, these results indicate that the order of the catalytic efficiency for the CO and CH<sub>4</sub> formation (onset potential and FE) is SaU-900 > SaU-800 > SaU-700, and SaU-800 > SaU-900 > SaU-700, respectively. The highest current density (Fig. 1c) at 6 h on SaU-900 indicates its best efficiency as the CO<sub>2</sub> reduction catalyst. It is important to mention that in the control experiments on bare titanium foil no formation of CO or CH<sub>4</sub> was detected in the tested potential range.

To study the stability of the catalysts for CO<sub>2</sub>ERR, the materials were tested at –0.75 V vs. RHE for 48 h. Fig. 2a and b show the trends for CO and CH<sub>4</sub> formations on both SaU-800 and SaU-900. The FE of CO increased from 4% (1 h) to 21% for SaU-900 and from 4% to 15% for SaU-800 within the first 6 h, and then remained stable throughout the whole reduction process. This behavior suggests that the catalysts were still active for CO formation even after the two-day reduction process. On the other hand, the FE of CH<sub>4</sub> on both SaU-800 and SaU-900 reached its maximum after 6 h and then decreased. When SaU-700 was used as a catalyst for 48 h, there were only small amounts of CO (2%) and CH<sub>4</sub> (0.02%) detected.

Based on the discussed performance above, the SaU-900 sample is the best catalyst, and it was therefore further used for a four-day reduction process (96 h). As shown in Fig. 2c, FE of CO still remained at the 15% level. This is the best stability among all nanoporous carbons we have studied so far [6,7]. For wood-based carbon [7], the FE of CO

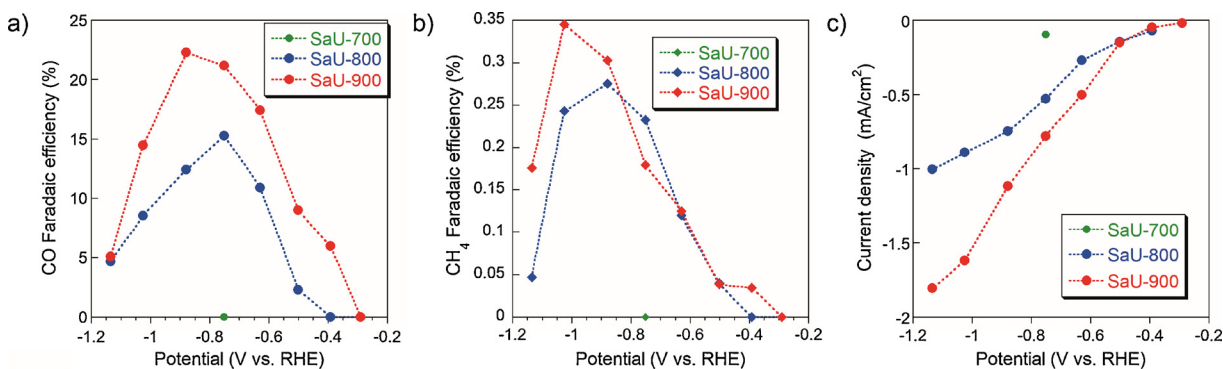


Fig. 1. Faradaic efficiency of CO (a) and CH<sub>4</sub> formation (b) and stationary CO<sub>2</sub> electrochemical reduction current density for samples studied at different potentials at 6 h reduction (c).

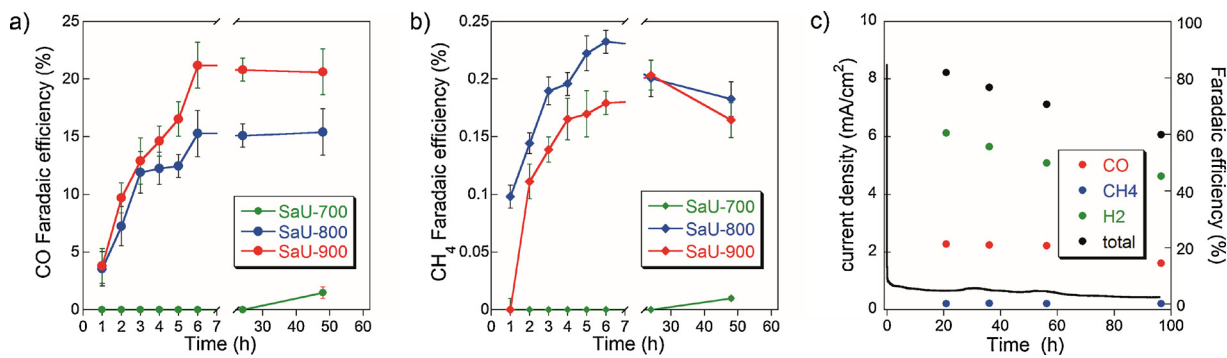


Fig. 2. Faradaic efficiency for CO (a) and CH<sub>4</sub> formation (b) during CO<sub>2</sub> reduction at the potential  $-0.75$  V vs. RHE; c) current density and FE for the detected gas phase of SaU-900 for 4 days.

dropped from 39% (at 1 h) to 15% only after 48 h of the reduction process.

Since HER was a concurrent reaction with CO<sub>2</sub>ERR, the extent of hydrogen evolution reaction was tested on the best performing material SaU-900. As seen in Fig. 2c, the total Faradaic efficiency accounts for 80% at 6 h reduction and still 20% of Faradaic efficiency remains unaccounted. As discussed previously [7], this might be due to the capacitive charging behavior of nanoporous carbons, the adsorption of the reduction products in pores, and the presence of dissolved products in the electrolyte that cannot be accounted for.

In order to verify the formation of the liquid products, NMR analysis of the electrolyte after CO<sub>2</sub> reduction for 48 h was carried out on all electrolytes. The <sup>1</sup>H NMR spectra along with the background spectrum of the electrolyte are presented in Fig. 3. A trace amount of C<sub>1</sub> products (methanol, formic acid) and C<sub>3</sub> products (acetone, propanol) were detected in the electrolytes of SaU-800 and SaU-900. Since all experiments were run following the same procedure, it was assumed that the difference in the amounts of the products formed could be evaluated semiquantitatively based on the comparison of the intensity of the specific peaks on the spectra. Thus, interestingly, the amounts of the liquid products formed on SaU-800 seem to be much higher than those on SaU-900. This, combined with more CH<sub>4</sub> detected in the headspace of the former sample, indicates that SaU-800 is a more efficient catalyst

for the hydrocarbons formation than is SaU-900. The amounts of the liquid products were not evaluated precisely (using calibration) since our target compounds are CO and CH<sub>4</sub> detected in the gas phase. Nevertheless, these results help us to partially resolve the balance of the current delivered to the system. After 4-day reduction, the total FE (including only CO, CH<sub>4</sub> and H<sub>2</sub>) decreased to 60%. It might be due to more unaccounted liquid products formed or/and slight imperfections in the sealing of the electrochemical cell, which might result in a leakage of hydrogen gas. Similar limitation for accounting the 100% of FE was also reported in other airtight systems [15].

The decomposition of the carbon catalysts themselves, which could result in the formation of CO or CH<sub>4</sub> was tested under N<sub>2</sub> saturated electrolyte at  $-0.75$  V vs. RHE. As shown in Fig. 4, all SaU samples were chemically very stable and very small amounts of CO were first detected only after 48 h reduction. The SaU-900 sample, which showed the best performance for CO<sub>2</sub>ERR, released the least CO (FE 0.33%). On SaU-700, the FE for CO formation after the 48 h reduction process was 1.5%. A trace amount of CH<sub>4</sub> was detected on all SaU samples. Here SaU-800 showed the highest degree of the composition with the FE of methane formation of 0.02% at 24 h and 0.025% at 48 h, which is much smaller than that on the wood-based carbon (0.06% at 48 h) [7]. The amounts of CO and CH<sub>4</sub> released from the carbons during the reduction in the N<sub>2</sub> saturated electrolyte were almost negligible comparing to

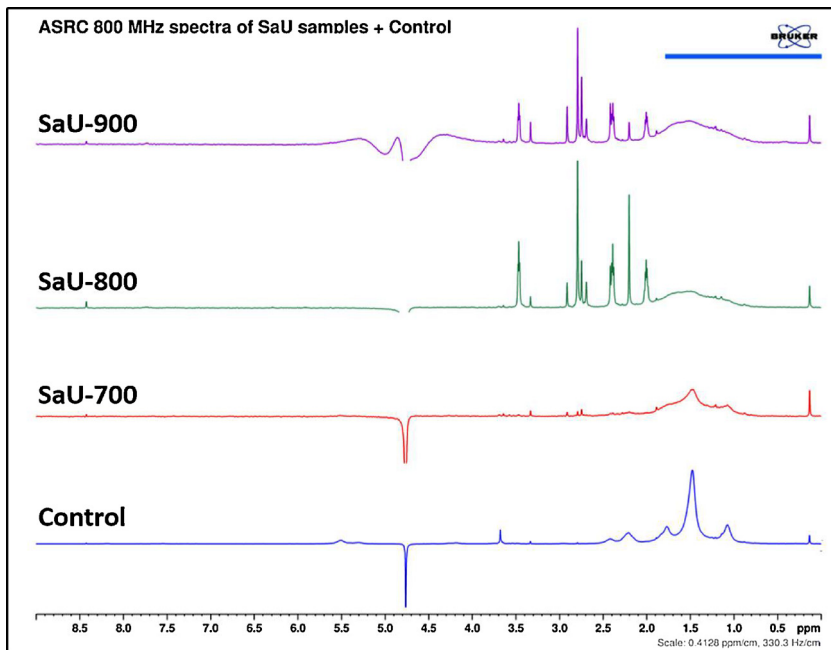
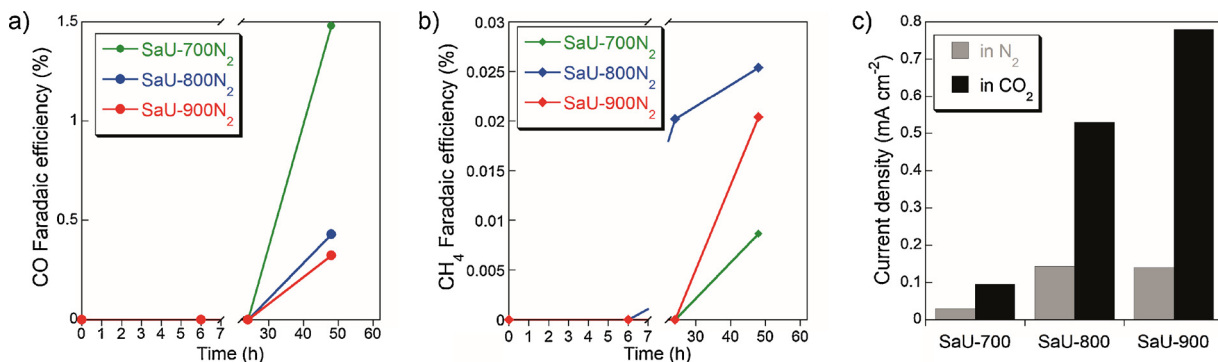


Fig. 3. NMR spectra of 0.1 M KHCO<sub>3</sub> electrolyte solutions before and after CO<sub>2</sub>ERR with 5% D<sub>2</sub>O (in the same scale). The control is CO<sub>2</sub> saturated 0.1 M KHCO<sub>3</sub> with 5% D<sub>2</sub>O. The peaks at 2.22(s), 3.34(s), 3.44(tri) and 8.33(s) correspond to acetone, methanol, propanol, formic acid, respectively.



**Fig. 4.** Faradaic efficiency for the CO (a) and CH<sub>4</sub> formation (b) in N<sub>2</sub>-saturated electrolyte and c) The comparison of the current densities in N<sub>2</sub> and CO<sub>2</sub> saturated electrolytes at the potential -0.75 V vs. RHE for the samples studied.

those formed in CO<sub>2</sub>ERR. Thus, the surface of SaU samples series is least susceptible for decomposition when exposed to reducing current among all nanoporous carbons we have tested so far.

### 3.2. Effect of surface features on CO<sub>2</sub>ERR

The porosity of the final carbon samples was measured using nitrogen adsorption. The isotherms on all materials reveal a high nitrogen gas uptake in the low relative pressure range, which indicates mainly microporous structures (Fig. S1 and Table S1 of the Supporting Information). All initial carbon samples exhibit high surface areas (Table S1). The SaU-700 sample, which was obtained at the lowest synthesis temperature, has the highest porosity (Fig. 1S, Table S1). Since for CO<sub>2</sub> reduction the carbons were mixed with binder (PVDF) and carbon black (CB), the porosity of actual electrodes was measured and used in the discussion. The results are presented in Fig. 5 and Table 1. The additives decreased the surface area not only owing to

their nonporous nature (20% decrease would be expected owing to the "dilution factor") but they also penetrated the pore structure. Nevertheless, the same trend in the differences in porosity as that for the as received carbons is preserved in the electrode materials. Interestingly, the SaU-900 electrode shows the presence of the smallest pores compared to other two electrodes and in these pores CO<sub>2</sub> adsorption forces should be the strongest.

The nanopores of the catalysts should be accessible to CO<sub>2</sub>/CO/H<sub>2</sub> molecules but not possibly for a large molecule of K<sub>3</sub>Fe(CN)<sub>6</sub>, so the electrochemically active surface area (ECSA) could not be accurately measured by the chronocoulometry of K<sub>3</sub>Fe(CN)<sub>6</sub> method. While the size of nitrogen molecule is similar to that of CO<sub>2</sub> ( $\sigma_{N_2} = 0.36$  nm;  $\sigma_{CO_2} = 0.33$  nm) and they can enter the majority of micropores with the predominant sizes less than 1 nm, the majority of active pores where CO<sub>2</sub> reduction can take place are not accessible to bulky ferro/ferri-cyanide ions of K<sub>3</sub>Fe(CN)<sub>6</sub> used as electrochemical standard with a size of about 1.1 nm [16,17]. Therefore, the effective surface area was

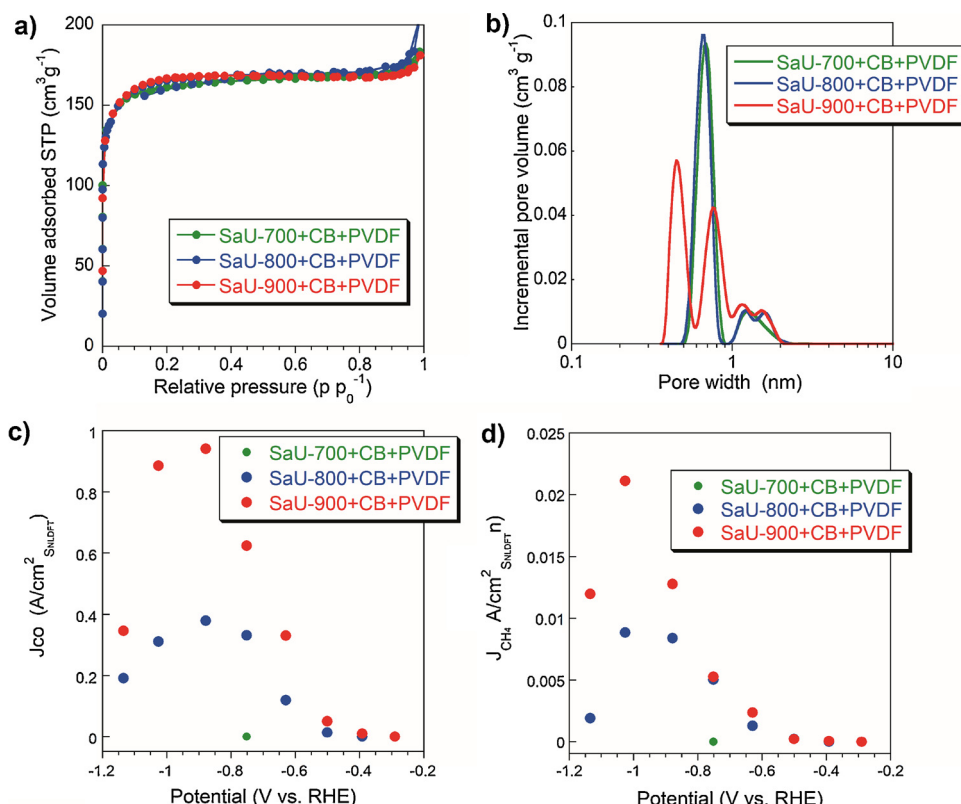


**Fig. 5.** a) Nitrogen adsorption isotherms on SaU-700/-800/-900 with 10 wt.% CB and 10 wt.% PVDF at -196 °C; b) Pore size distributions; c) Dependence of the normalized current density related to CO formation on the potential; d) Dependence of the normalized current density related to CH<sub>4</sub> formation on the potential.

**Table 1**

The parameters of the porous structure for the electrode materials studied.

Electrode (SaU + CB + PVDF)	$S_{\text{NLDFT}}$ ( $\text{m}^2/\text{g}$ )	$V_t$ ( $\text{cm}^3/\text{g}$ )	$V_{\text{meso}}$ ( $\text{cm}^3/\text{g}$ )	$V_{<0.7\text{ nm}}$ ( $\text{cm}^3/\text{g}$ )	$V_{<1\text{ nm}}$ ( $\text{cm}^3/\text{g}$ )	$V_{\text{mic}}$ ( $\text{cm}^3/\text{g}$ )	$V_{\text{mic}}/V_t$
SaU-700	596	0.283	0.052	0.101	0.173	0.231	0.82
SaU-800	610	0.317	0.081	0.120	0.167	0.237	0.75
SaU-900	662	0.280	0.028	0.085	0.166	0.248	0.89

directly calculated from the weight of the electrode materials. The effective surface areas for SaU-700, SaU-800 and SaU-900 are  $4.77 \text{ m}^2$ ,  $4.88 \text{ m}^2$  and  $5.30 \text{ m}^2$ , respectively. Fig. 5c and 5d show the dependence of the current density normalized per unit surface area on the potential. As seen, SaU-900 outperforms SaU-800 between  $-0.6 \text{ V}$  to  $-1 \text{ V}$  vs. RHE in the processes of CO and  $\text{CH}_4$  formation.

As seen from Table S1 of the Supporting Information, micropores constitute between 92 and 94% of the total pore volumes of our electrode samples. SaU-800 with CB and PVDF, which showed the highest ratio of the FE of hydrocarbon formation to that of CO formation, has a higher ultramicropore volume (~42%) than has SaU-900 with CB and PVDF. This result suggests that the smallest pores of carbons might be beneficial for the hydrocarbon formation. It was also a hypothesis formulated in our previous work, where we indicated that ultramicropores might work as Fisher-Tropsch nanoreactors promoting methane formation [7]. Indeed, also in this study a higher  $\text{CH}_4/\text{CO}$  ratio was found on SaU-800 than on SaU-900, which we link to the higher volume of ultramicropores of the former sample. Another important factor that influences the  $\text{CO}_2\text{ERR}$  is the electrical conductivity. Although SaU-700 shows the highest surface area among all samples tested, it showed the lowest catalytic activity for  $\text{CO}_2\text{ERR}$ . That dramatic difference in the FE can be linked to the differences in the DC conductivity. Table S1 includes the resistance of each material coated on a gold interdigitated chip. The resistance of SaU-700 is three orders of magnitude higher than that of SaU-800. It is well known that the conductivity of amorphous carbon increases with an increase in the level carbon graphitization and in the sizes of  $\text{sp}^2$  units and both increase with an increase in carbonization temperature [18,19]. Eventually, the low conductivity of the SaU-700 sample might hinder the reduction process, which involves an electron transfer to the electrode surface, one of the factors driving the reduction reactions. The lower the conductivity of a material, the lower is the electric current transferred in the reduction system. Thus, the smallest current density of SaU-700 in the  $\text{N}_2$  saturated electrolyte, in spite of its favorable porous structure, can be linked to its limited electric conductivity.

Furthermore, the surface chemistry of the sample is also expected to affect the  $\text{CO}_2$  reduction process. Therefore, the surface chemistry of the initial carbons was studied using potentiometric titration (Table 2, Fig. S2 of the Supporting Information). Table 2 summarizes the distributions of the acidity constants of the species detected on the carbon surfaces along with the average surface pH values. Among the three samples tested, SaU-700 showed the highest pH, i.e. the lowest acidity. SaU-800 and SaU-900 have similar surface pH values. The amount of strong acid groups on the surface of SaU-800 (0.373 mmol/g) is higher than that on SaU-900 (0.120 mmol/g). An increase in the carbonization temperature resulted in a decrease in the numbers of carboxylic groups, which is attributed to the generally occurring higher degree of carbonization with an increasing temperature. Since SaU-800 showed the higher extent of hydrocarbon formation and the worse FE of CO formation than

**Table 3**

Atomic concentrations of elements on the surface determined by XPS analysis. E – the samples after  $\text{CO}_2$  reduction;  $\text{N}_2$  – the sample after reduction in the nitrogen saturated electrolyte.

Sample	Element content [at. %]		
	C	O	N
SaU-700	70.0	19.1	10.9
SaU-700E	81.1	10.7	8.2
SaU-800	75.0	14.4	10.6
SaU-800E	84.5	11.0	4.5
SaU-900	80.2	14.6	5.2
SaU-900E	82.7	15.0	2.3
SaU-900N <sub>2</sub>	86.4	11.0	2.6

that of SaU-900, the smaller catalytic activity of the former sample for the CO formation might be liked to its surface acidity, which promotes HER, as a competing reaction [6,7]. On the other hand, the strong acidic surface might help with the protonation reaction and thus with the hydrocarbon formation.

XPS analysis was performed on the initial carbons and those after  $\text{CO}_2\text{ERR}$  at  $-0.75 \text{ V}$  vs. RHE for 48 h. The latter are referred to with letter E. As seen from Table 3, the synthesis of the carbon at  $900^\circ\text{C}$  resulted in the material with the smallest content of nitrogen, which is half of that on SaU-700 and SaU-800. The elemental analysis shows the similar trends (Table S2 of the Supporting Information), however, some differences in the elemental content suggest that more nitrogen is apparently present in the bulk than on the surface (XPS detects elements on the surface up to 0.7 nm in depth). Besides nitrogen, also oxygen is present which does not show significant differences in its content on the surface of SaU-800 and SaU-900. Knowing that even trace amounts of metals can catalyze  $\text{CO}_2$  reduction, the content of zinc on the surface was determined and found to be 0.26 at. %, 0.52 at. % and 0.55 at. % for SaU-700, SaU-800 and SaU-900, respectively. Since both SaU-800 and SaU-900 have similar zinc content, the enhanced activity on the latter sample should not be linked to this impurity. Metal impurities (Ni, Fe, Mn, and Cu) in graphite, graphene oxide and carbon nanotubes have been systematically studied as affecting the activity for  $\text{CO}_2$  reduction [20]. However, the trace amounts of zinc have not been reported as catalytically active for  $\text{CO}_2$  reduction, to the best of our knowledge.

The detailed deconvolution of C 1s, O 1s, N 1s core energy level spectra (Fig. S3, S4 of the Supporting Information, Fig. 6) revealed the differences in specific configurations of the surface groups. As expected, SaU-900 shows the highest level of carbonization and the smallest contribution of carbon-oxygen bonds. The most oxidized sample is SaU-700. This is confirmed by the deconvolution results of O 1s core energy level spectra. They are consistent with those from potentiometric titration, which showed the smallest amount of strong acidic groups (mostly carboxylic groups) on the surface SaU-900 (Table 2, Fig. S3 and

**Table 2**

Surface pH values, peak positions and numbers of groups (in parentheses, [mmol/g]) for the material studied.

Sample	Surface pH	pK <sub>a</sub> 4-5	pK <sub>a</sub> 5-6	pK <sub>a</sub> 6-7	pK <sub>a</sub> 7-8	pK <sub>a</sub> 8-9	pK <sub>a</sub> 9-10	pK <sub>a</sub> 10-11	All Groups	Adic groups (pK <sub>a</sub> < 7)
SaU-700	4.37	4.30 (0.257)	5.43 (0.082)	6.08 (0.108)	7.58 (0.168)	8.94 (0.205)	9.91 (0.413)		1.232	0.447
SaU-800	3.80	4.41 (0.210)	5.95 (0.163)		7.56 (0.450)		9.36 (0.343)	10.62 (0.303)	1.470	0.373
SaU-900	3.59	4.42 (0.120)			7.67 (0.772)		9.87 (0.233)		1.126	0.120

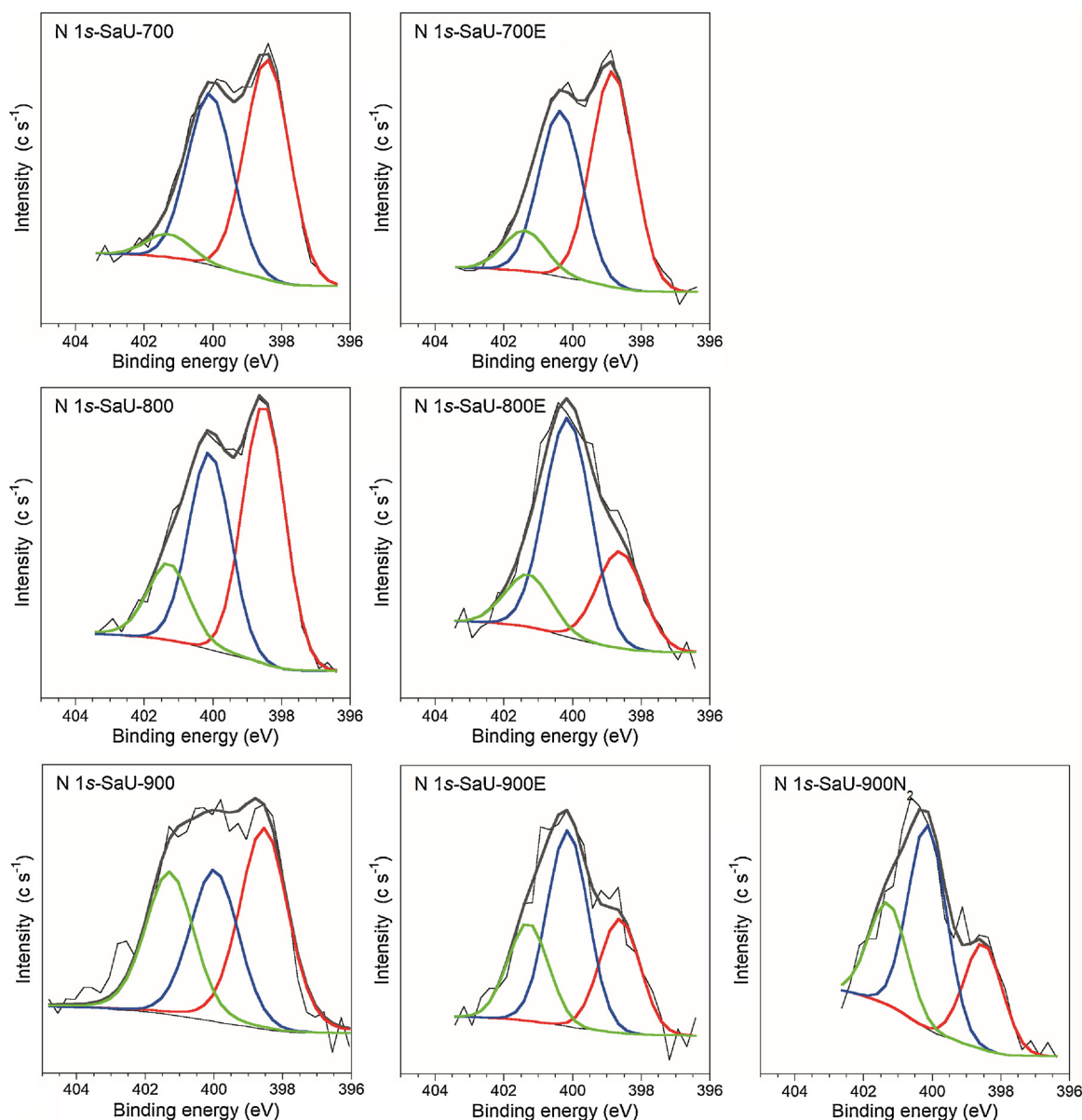


**Fig. 6.** N 1s core energy level spectra of the initial and exhausted SaU samples.

**Table 4**

The results of deconvolution of C 1s, O 1s and N 1s core energy level spectra for the materials studied.<sup>a</sup> They are reported as received (in parentheses) and adjusted to the total content of a particular element. E denotes the samples after CO<sub>2</sub> reduction and N<sub>2</sub> – the sample after reduction in the nitrogen saturated electrolyte.

Energy, eV	Bond assignment	SaU-700	SaU-700E	SaU-800	SaU-800E	SaU-900	SaU-900E	SaU-900N <sub>2</sub>
<b>C 1s</b>								
284.8–284.9	C–C ( <i>sp</i> <sup>2</sup> , graphitic carbon)	47.4 (67.7)	40.9 (50.3)	51.1 (68.1)	47.8 (56.6)	53.3 (66.4)	50.9 (61.5)	50.3 (58.2)
286.0–286.4	C–O(phenolic, alcoholic, etheric), C–N configurations	19.3 (27.6)	22.0 (27.1)	20.4 (27.2)	24.9 (29.5)	18.0 (22.5)	21.1 (25.4)	21.3 (24.7)
287.0–287.1	C=O (carbonyl or quinone)		14.6 (18.0)		9.2 (10.9)	6.7 (8.4)	10.0 (12.1)	12.6 (14.6)
288.1–288.5	O=C=O (carboxyl or ester)	3.3 (4.7)	3.7 (4.6)	3.6 (4.8)	2.5 (3.0)	2.2 (2.8)	0.8 (1.0)	2.2 (2.5)
<b>O 1s</b>								
531.0–531.5	O=C (in carboxyl/carbonyl) or O=N	1.2 (6.1)	1.5 (13.9)	2.0 (13.7)	3.1 (28.4)	1.7 (11.5)	1.4 (9.3)	1.6 (14.2)
532.4–532.7	O–C (in phenol/epoxy/ether) or O–N	16.5 (86.4)	5.7 (53.2)	10.4 (72.4)	5.5 (49.7)	9.8 (67.1)	8.3 (55.5)	6.2 (56.3)
533.3–533.6	–O– (water or chemisorbed oxygen species), Occluded CO or CO <sub>2</sub>	1.4 (7.5)	3.5 (33.0)	2.0 (13.9)	2.4 (21.9)	3.1 (21.4)	5.3 (35.2)	3.2 (29.5)
<b>N 1s</b>								
398.5–398.8	N1 (in pyrazines/pyridines)	5.8 (53.0)	4.2 (51.1)	5.1 (47.6)	1.2 (26.3)	2.0 (38.2)	0.6 (28.0)	0.7 (25.9)
400.1–400.4	N2 (in pyrroles/pyridones)	4.5 (41.4)	3.2 (39.3)	3.6 (33.8)	2.7 (59.5)	1.7 (33.3)	1.1 (48.0)	1.3 (49.3)
401.1–401.3	N3 (in quaternary-N)	0.6 (5.6)	0.8 (9.6)	1.9 (18.6)	0.6 (14.2)	1.5 (28.5)	0.6 (24.0)	0.6 (24.8)

<sup>a</sup> The contribution from fluorine to the carbon 1s XPS spectrum has been subtracted.

S4).

The deconvolution of N 1s core energy level spectra (Table 4, Fig. 6) show changes/decrease in all the contributions for SaU-900 compared to the other two samples. This indicates that 900 °C is a critical synthesis temperature resulting in the dramatic change in carbon chemistry. Even though pyrazinic-N and pyridinic-N have the same binding energy and based on XPS analysis these two species cannot be distinguished, it was previously suggested that an increase in the carbonization temperature of the pre-organized precursor (it was squaric acid and urea in our case) [10,11] caused the gradual conversion of pyrazinic moieties into pyridinic ones. Based on this, it is assumed that a decrease in N1 nitrogen in SaU-900 could be caused by the decomposition of the pyrazinic nitrogen. This was followed by a change in the nitrogen environment and its incorporation in the quaternary form to the carbon matrix. The contribution of quaternary-N increased with the increase in the synthesis temperature. It was expected due to the conversion of other, less thermally stable, nitrogen groups to the quaternary ones at high temperatures [17,18].

After CO<sub>2</sub>ERR, the contents of nitrogen and oxygen markedly decreased. This is interesting since our previous study on nitrogen-modified carbons showed that the overall content of nitrogen did not change, although its speciation on the surface was altered [6,7]. These results suggest the difference in the catalytic mechanism between the carbons addressed in this study and those previously reported, probably caused by the specific surface features of the former ones. As mentioned above, one of the nitrogen containing species which might exist on the surface of our carbons is pyrazinic-N [10,11]. The electrochemical study of pyridine and pyrazine indicated that the pyrazine ring is much easier to be reduced than is the pyridine one [23,24]. Even though we are not able to clearly separate/distinguish the contribution of pyrazinic nitrogen from that of pyridinic, the observed decrease in nitrogen content upon CO<sub>2</sub> reduction might be caused by the decomposition of pyrazinic-N. The surface reduction of this species during CO<sub>2</sub>ERR is especially visible for the most conductive SaU-800 and SaU-900 samples.

The CO<sub>2</sub> reduction for 48 h resulted in the unchanged activity for the CO formation on both SaU-800 and SaU-900, as discussed above. This indicates that the catalytically active sites for CO<sub>2</sub> reduction to CO, which are likely pyridinic-N configurations [6,7] are not consumed during CO<sub>2</sub>ERR. The previous studies showed an increase of pyridonic-N nitrogen after CO<sub>2</sub>ERR. The formation of pyridonic-N species was caused by the oxidation of a positively charged carbon in the pyridinic configuration during the CO<sub>2</sub> reduction process. However, the trend in surface chemistry observed here differs from the previously reported results [6,7] and rather a decrease in the contribution of pyridones is found after CO<sub>2</sub>ERR. Thus the stability and the surface chemistry analyses suggest that the oxidation of pyridinic-N did not take place during 48 h of the CO<sub>2</sub> reduction. The trend found in this study could be due to the reactivity of pyrazinic-N. Even though these species are not very active in the CO formation, they might work as sacrificial agents, which undergo oxidation shielding in this way the catalytically active pyridines from oxidation. This leads to the good performance/high catalyst stability during the CO<sub>2</sub>ERR process. It is noted, that surface oxidation always occurs to some extent during the applications of carbons as CO<sub>2</sub> reduction catalyst.

While oxygen in SaU-900 is rather stable after the CO<sub>2</sub> reduction in terms of its amount and speciation, a marked reduction of oxygen content is observed on the surface of the samples obtained at 700 and 800 °C. It is likely caused by a cathodic current, and these results once again show the differences in the surface chemistry stability of the samples tested. In addition, the amount of oxygen on SaU-900 after 48 h reduction in saturated N<sub>2</sub> electrolyte is smaller than that in saturated CO<sub>2</sub> electrolyte owing to slight surface oxidation during the CO<sub>2</sub> reduction process, as discussed above.

Another important and unique finding on the SaU carbons is the detection of C<sub>3</sub> hydrocarbon products (acetone and propanol) in the

liquid phase (Fig. 3). The overpotential for the C<sub>2+</sub> hydrocarbon formation for both SaU-800 and SaU-900 is much lower than the overpotential reported on copper foil where acetone and propanol were formed at −0.95 V vs. RHE [21,22]. The previous studies suggested that the micropore volume, especially the ultra-micropore volume is crucial for the hydrocarbon formation [6,7]. Strong CO adsorption in the pore system in the presence of adsorbed hydrogen from water splitting was indicated as a possible mechanism for its further reduction to CH<sub>4</sub>. The effect of the strength of the adsorption process might be demonstrated in the higher Faradaic efficiency of the hydrocarbons formation on SaU-800 than that on SaU-900 (Fig. 2b and Fig. 3). Although the results suggest that pyrazinic-N might not be as active as pyridinic-N for CO formation from CO<sub>2</sub>, the formed CO in the pores could be stabilized/strongly adsorbed in the vicinity of the pyrazinic-N configurations in SaU-800. This scenario is a hypothetical one since, as indicated above we were not able to differentiate between pyrazinic and pyridinic-N, based on XPS analysis. These interactions might be governed by the polarity of formed CO and the attraction of its oxygen to the positive charge on carbon atom due to nitrogen incorporated to the carbon ring. If two CO\* intermediates were formed in close proximity in small pores, their reduction could lead to the formation of C–C bonds. The results also showed that the surface active sites of the SaU carbons catalyze the formation of a number of different C<sub>1</sub> oxygenates (forming CH<sub>4</sub>, then methanol and formic acid) and thus these diverse C<sub>1</sub> species could couple to form the C<sub>2+</sub> products. If the C–C coupling step between the various C<sub>1</sub> intermediates is kinetically possible [25,26], this could explain the C<sub>2+</sub> products detected.

The FE of CH<sub>4</sub> increased with the amount of quaternary-N present in SaU-800 and SaU-900. Both samples have much higher electrical conductivity than has SaU-700. Quaternary nitrogen is a positively charged site in the carbon network, and in this form it can exist even in the walls of very small pores, especially ultramicropores. Thus these sites can contribute to strong CO\* adsorption in these pores via attraction of opposite charges [27,28]. This might further facilitate CO\* reduction and formation of methane in the reaction with adsorbed hydrogen [7]. A decrease in quaternary nitrogen after electrochemical reduction suggests the involvement of these species in the methane formation since oxygen released in this process might oxidize the quaternary nitrogen. The oxidation process of the catalytic centers can explain a decrease in the Faradaic efficiency of CH<sub>4</sub> formation, which is found with the progress of CO<sub>2</sub>ERR.

#### 4. Conclusions

In this study, the performance of high nitrogen-content microporous carbon in CO<sub>2</sub>ERR was investigated with emphasis on the role of nitrogen moieties incorporated to the carbon matrix. The materials obtained at 800 and 900 °C showed a long-durable performance with the 21% of Faradaic efficiency for CO formation. Even though that FE is not very high, the stability of the catalysts is remarkable. The results suggest that the small electrical conductivity of the sample synthesized at 700 °C might limit the CO<sub>2</sub>ERR. The changes in the nitrogen environments on the surface for the initial and used in CO<sub>2</sub> electroreduction samples, along with the history of the carbons (chemistry of precursors) suggest that pyrazinic-N might protect the active pyridinic nitrogen, which is the main catalytic center for CO<sub>2</sub> reduction to CO, from oxidation. Quaternary nitrogen is found to be active in CH<sub>4</sub> formation, since it is consumed during the CO<sub>2</sub> reduction process. In addition, the microporous structure favors the hydrocarbon formation. Since C<sub>3</sub> products were detected for the first time on the nanoporous carbons, the structural uniqueness of the pyrazinic-N (two N in a close proximity) in the microporous structure might promote the C–C bond-formation. This research indicated that not only specific chemical environment of nitrogen but also its location in the carbon matrix affect the CO<sub>2</sub> electroreduction process. The specific surface chemistry of the catalysts tested provides a distinctive selectivity of the products formed

and stability during the CO<sub>2</sub>ERR. Thus, the results obtained represent a marked advance in the development of nanoporous carbon-based CO<sub>2</sub> reduction catalysts. The findings have significant implications for the understanding of the CO<sub>2</sub> reduction process and functional nitrogen-carbon motives.

## Acknowledgments

This research was partially funded by NSF CBET Grant No. 1133112. <sup>1</sup>H NMR data presented herein were collected in part at the City University of New York Advanced Science Research Center (CUNY ASRC), Biomolecular NMR and XPS Facility.

## Appendix A. Supplementary data

Supplementary material related to this article can be found, in the online version, at doi:<https://doi.org/10.1016/j.apcatb.2018.04.021>.

## References

- [1] B. Kumar, M. Asadi, D. Pisasale, S. Sinha-Ray, B. a Rosen, R. Haasch, J. Abiade, A.L. Yarin, A. Salehi-Khojin, Renewable and metal-free carbon nanofibre catalysts for carbon dioxide reduction, *Nat. Commun.* 4 (2013) 2819–2826, <http://dx.doi.org/10.1038/ncomms3819>.
- [2] P.P. Sharma, J. Wu, R.M. Yadav, M. Liu, C.J. Wright, C.S. Tiwary, B.I. Yakobson, J. Lou, P.M. Ajayan, X.D. Zhou, Nitrogen-doped carbon nanotube arrays for high-efficiency electrochemical reduction of CO<sub>2</sub>: on the understanding of defects, defect density, and selectivity, *Angew. Chem. Int. Ed.* 54 (2015) 13701–13705, <http://dx.doi.org/10.1002/anie.201506062>.
- [3] J. Wu, R.M. Yadav, M. Liu, P.P. Sharma, C.S. Tiwary, L. Ma, X. Zou, X.-D. Zhou, B.I. Yakobson, J. Lou, P.M. Ajayan, Achieving highly efficient, selective, and stable CO<sub>2</sub> reduction on nitrogen-doped carbon nanotubes, *ACS Nano* 9 (2015) 5364–5371, <http://dx.doi.org/10.1021/acsnano.5b01079>.
- [4] J. Xu, Y. Kan, R. Huang, B. Zhang, B. Wang, K.-H. Wu, Y. Lin, X. Sun, Q. Li, G. Centi, D. Su, Revealing the origin of activity in nitrogen-doped nanocarbons towards electrocatalytic reduction of carbon dioxide, *ChemSusChem* 9 (2016) 1085–1089, <http://dx.doi.org/10.1002/cssc.201600202>.
- [5] H. Wang, Y. Chen, X. Hou, C. Ma, T. Tan, Nitrogen-doped graphenes as efficient electrocatalysts for the selective reduction of carbon dioxide to formate in aqueous solution, *Green Chem.* 18 (2016) 3169–3458, <http://dx.doi.org/10.1039/c6gc00410e>.
- [6] W. Li, M. Seredych, E. Rodríguez-Castellón, T.J. Bandosz, Metal-free nanoporous carbon as a catalyst for electrochemical reduction of CO<sub>2</sub> to CO and CH<sub>4</sub>, *ChemSusChem* 9 (2016) 606–616, <http://dx.doi.org/10.1002/cssc.201501575>.
- [7] W. Li, B. Herkt, M. Seredych, T.J. Bandosz, Pyridinic-N groups and ultramicropore nanoreactors enhance CO<sub>2</sub> electrochemical reduction on porous carbon catalysts, *Appl. Catal. B Environ.* 207 (2017) 195–206, <http://dx.doi.org/10.1016/j.apcatb.2017.02.023>.
- [8] Y. Hori, H. Konishi, T. Futamura, A. Murata, O. Koga, H. Sakurai, K. Oguma, “Deactivation of copper electrode” in electrochemical reduction of CO<sub>2</sub>, *Electrochim. Acta* 50 (2005) 5354–5369, <http://dx.doi.org/10.1016/j.electacta.2005.03.015>.
- [9] Q. Lu, J. Rosen, Y. Zhou, G.S. Hutchings, Y.C. Kimmel, J.G. Chen, F. Jiao, A selective and efficient electrocatalyst for carbon dioxide reduction, *Nat. Commun.* 5 (2014) 3242–3247, <http://dx.doi.org/10.1038/ncomms4242>.
- [10] N. Fechler, N.P. Zussblatt, R. Rothe, R. Schlogl, M.G. Willinger, B.F. Chmelka, M. Antonietti, Eutectic syntheses of graphitic carbon with high pyrazinic nitrogen content, *Adv. Mater.* 28 (2016) 1287–1294, <http://dx.doi.org/10.1002/adma.201501503>.
- [11] T. Jordan, M. Shalom, M. Antonietti, N. Fechler, Carbon nanoarchitectures by design: pre-organizing squaric acid with urea, *Asia-Pacific J. Chem. Eng.* 11 (2016) 866–873, <http://dx.doi.org/10.1002/api.2020>.
- [12] J. Jagiello, T.J. Bandosz, J.A. Schwarz, Application of inverse gas chromatography at infinite dilution to study the effects of oxidation of activated carbons, *Carbon* 30 (1992) 63–69.
- [13] J. Jagiello, J.P. Olivier, Carbon slit pore model incorporating surface energetical heterogeneity and geometrical corrugation, *Adsorption* 19 (2013) 777–783, <http://dx.doi.org/10.1007/s10450-013-9517-4>.
- [14] Y. Hori, Electrochemical CO<sub>2</sub> reduction on metal electrodes, *Mod. Asp. Electrochem.* (2008) 89–189, [http://dx.doi.org/10.1007/978-0-387-49489-0\\_3](http://dx.doi.org/10.1007/978-0-387-49489-0_3).
- [15] T. Yamamoto, D.A. Tryk, K. Hashimoto, A. Fujishima, M. Okawa, Electrochemical reduction of CO<sub>2</sub> in the micropores of activated carbon fibers, *J. Electrochem. Soc.* 147 (2000) 3393–3400, <http://dx.doi.org/10.1149/1.1393911>.
- [16] Y. Morioka, K. Toriumi, T. Ito, A. Saito, I. Nakagawa, Crystal structures of the room- and low-temperature phases of monoclinic potassium ferricyanide, *J. Phys. Soc. Jpn.* 54 (1985) 2184–2189, <http://dx.doi.org/10.1143/JPSJ.54.2184>.
- [17] B.N. Figgis, M. Gerloch, R. Mason, The crystallography and paramagnetic anisotropy of potassium ferricyanide, *Proc. R. Soc. A Math. Phys. Eng. Sci.* 309 (1969) 91–118, <http://dx.doi.org/10.1098/rspa.1969.0031>.
- [18] J. Robertson, Mechanical properties and coordinations of amorphous carbons, *Phys. Rev. Lett.* 68 (1992) 220–223, <http://dx.doi.org/10.1103/PhysRevLett.68.220>.
- [19] J. Robertson, E.P. O'Reilly, Electronic and atomic structure of amorphous carbon, *Phys. Rev. B* 35 (1987) 2946–2957 (accessed March 21, 2018), <http://www.ncbi.nlm.nih.gov/pubmed/9941778>.
- [20] Y. Lum, Y. Kwon, P. Lobaccaro, L. Chen, E.L. Clark, A.T. Bell, J.W. Ager, Trace levels of copper in carbon materials show significant electrochemical CO<sub>2</sub> reduction activity, *ACS Catal.* 6 (2016) 202–209, <http://dx.doi.org/10.1021/acs.catal.5b02399>.
- [21] H. Schmiers, J. Friebel, P. Streubel, R. Hesse, R. Köpsel, Change of chemical bonding of nitrogen of polymeric N-heterocyclic compounds during pyrolysis, *Carbon* 37 (1999) 1965–1978, [http://dx.doi.org/10.1016/S0008-6223\(99\)00071-8](http://dx.doi.org/10.1016/S0008-6223(99)00071-8).
- [22] B. Xiao, J.P. Boudou, K.M.M. Thomas, Reactions of nitrogen and oxygen surface groups in nanoporous carbons under inert and reducing atmospheres, *Langmuir* 21 (2005) 3400–3409, <http://dx.doi.org/10.1021/la0472495>.
- [23] S. Roffia, M. Marcaccio, C. Paradisi, F. Paolucci, V. Balzani, G. Denti, S. Serroni, S. Campagna, Electrochemical reduction of (2,2'-Bipyridine) and bis((2-Pyridyl)pyrazine)ruthenium(II) complexes used as building-blocks for supramolecular species - redox series made of 8, 10, and 12 redox steps, *Inorg. Chem.* 32 (1993) 3003–3009.
- [24] B.J. Tabner, J.R. Yandler, A correlation of half-wave reduction potentials with theoretical calculations for some nitrogen-containing heteromolecules in dimethyl-formamide, *Inorg. Phys. Theor.* (1968) 381–388.
- [25] K.P. Kuhl, E.R. Cave, D.N. Abram, T.F. Jaramillo, E. Environ, New insights into the electrochemical reduction of carbon dioxide on metallic copper surfaces, *Energy Environ. Sci.* 5 (2012) 7050–7059, <http://dx.doi.org/10.1039/c2ee21234j>.
- [26] S. Sen, D. Liu, G.T.R. Palmore, Electrochemical reduction of CO<sub>2</sub> at copper nanofoams, *ACS Catal.* 4 (2014) 3091–3095, <http://dx.doi.org/10.1021/cs500522g>.
- [27] A. Zecchina, S. Bordiga, G. Spoto, D. Scarano, M. Padovan, O. Arean, Low-temperature fourier-transform infrared investigation of the interaction of CO with nanosized ZSM5 and silicalite, *J. Chem. Soc. Faraday Trans.* 88 (1992) 2959–2969.
- [28] S. Bordiga, C. Lamberti, F. Geobaldo, A. Zecchina, G.T. Palomino, C.O. Arean, Fourier-Transform infrared study of CO adsorbed at 77 K on H-mordenite-mordenite and alkali-metal-exchanged mordenites, *Langmuir* 11 (1995) 527–533, <http://dx.doi.org/10.1021/la00002a027>.